Toward Understanding the Causes of Low-Frequency Variability: The Interannual Standard Deviation of Monthly Mean 700-mb Height

ANTHONY G. BARNSTON AND HUUG M. VAN DEN DOOL

Climate Analysis Center, NMC/NWS/NOAA, Washington, D.C.

(Manuscript received 18 June 1992, in final form 31 March 1993)

ABSTRACT

The field of standard deviation of monthly mean 700-mb geopotential height in the Northern Hemisphere for each of the 12 months over the 1950–1991 period, among other auxiliary statistics, is compiled in an atlas to which this paper is companion. Some of the major features found in the atlas are highlighted and extended here. A comparison is also made to the same statistics derived from a 10-year run of the NMC model.

There are three distinct regions of peak standard deviation (up to 85 geopotential meters in winter), all of which are located over water. Two of them remain positionally relatively stationary throughout the year in the high-latitude Pacific and Atlantic oceans, respectively. A portion of the Pacific region's winter variability comes from interdecadal fluctuations. The third region is over the Arctic Ocean and exhibits some large seasonal changes in location. A roughly north-to-south troughlike minimum in standard deviation (down to less than 20 geopotential meters in summer) is found in west central North America throughout most of the year.

The standard deviation maxima (minima) coincide largely with areas with a high (low) frequency of occurrence of height anomaly centers of both signs. Many of these anomaly centers occur in spatial coherence with other centers, forming familiar teleconnection and principal component patterns. While the high (low) standard deviation areas invest greater (lesser) amounts of variance in these coherent variability clusters than the surrounding regions, their involvement in terms of the strength of the relationships is not substantially greater (smaller). The standard deviation field does not move north and south with the changes in season as do the jets, storm tracks, and the mean flow. In summer the standard deviation peaks are largely detached from spatially coherent variability patterns, suggesting that they may be caused in large part by local interactions related to permanent (spatially fixed) features of the lower boundary at all times of the year.

The observed monthly mean 700-mb flow and the quasi-stationary locations of its interannual standard deviation maxima and minima are reproduced in approximate form in a 10-year run of the NMC medium-range forecast model. This helps provide evidence that the field of standard deviation is related, directly or indirectly, to some of the geographically fixed boundary conditions across the globe such as SST, ocean–land interfaces, and terrain.

1. Introduction

The behavior of the upper-air, monthly mean planetary-scale circulation is of interest to meteorologists both from a purely physical and a predictive standpoint. Many studies have attempted to characterize this behavior in terms of preferred flow patterns (Wallace and Gutzler 1981; Namias 1981; Horel 1981; Esbensen 1984; Barnston and Livezey 1987), persistence of the flow (Namias 1952; Van den Dool and Livezey 1984), and the correspondence to the climate at the surface (Klein 1983; Klein and Walsh 1983). In this paper we look at the interannual standard deviation of monthly mean 700-mb height for each of the 12 months in the extratropical Northern Hemisphere over the 1950–1991 period. This simple quantity is relevant to a wide variety of studies and applications and should be available to the research community as well as climatologists and operational meteorologists for guidelines for prediction (e.g., where to place anomaly centers or "zero lines"); yet it is often difficult to acquire readily. Because large volumes of maps are inappropriate for scientific journals, we are publishing them in an atlas (Barnston and Van den Dool 1993). The present paper highlights and extends some of the more interesting features of the maps found in the atlas, and strikes a comparison to data generated in a 10-year model run made at NMC (Van den Dool et al. 1991).

The application of a monthly mean filter to daily 700-mb height data removes most, if not all, of the high-frequency variability (i.e., individual weather systems associated with baroclinic eddies), resulting in a description of the low-frequency variability that applies to long-range forecasts such as those issued at the Climate Analysis Center (CAC) of the National Meteorological Center (NMC). In examining the low-frequency component of the geopotential height variability, it should be kept in mind that there is

Corresponding author address: Dr. Anthony G. Barnston, Climate Analysis Center, NMC/NWS/NOAA, W/NMC 51, WWB RM 604, Washington, DC 20233.

continuous two-way feedback between the high- and low-frequency variability (i.e., phenomena occurring on the synoptic and the planetary spatial scales, respectively), and that the low-frequency variability alone does not constitute a closed system (Cai and Mak 1990; Wallace 1987). In this feedback system the low-frequency variability (the planetary waves) encourages high-frequency eddy development downstream of the long-wave troughs, and the eddies (synoptic weather systems) reinforce certain aspects (i.e., the barotropic component) of the existing long-wave patterns. The planetary waves and the associated storm tracks downstream of the large-scale troughs may all be in general motion throughout this symbiotic process (Cai and Van den Dool 1991). In other cases, long-lived anomaly structures and their high-frequency counterparts grow and decay in one general location.

A monthly mean filter may not be desirable to all researchers. However, as shown by Blackmon et al. (1984), the field of root-mean-square departure from the mean of bandpass-filtered geopotential heights is very similar to the field of the standard deviation of monthly mean heights. Upon initial inspection the monthly mean time filter removes virtually all high-frequency baroclinic variations. One must keep in mind, though, that Madden (1976) showed that the majority of the standard deviation of monthly means is due to the effects of day-to-day variability. Madden's sampling approach is the statistical companion of the dynamical high- versus low-frequency interaction theory.

The causes of atmospheric low-frequency variability at midlatitudes are not well known. There are speculations about their origin, which can be classified into two broad categories. The first of these is an atmospheric response to anomalous long-lived external forcing (Opsteegh and Van den Dool 1980), such as tropical sea surface temperature (SST) anomalies during ENSO (Cane and Zebiak 1987; Ropelewski and Halpert 1986). The second category is the internal dynamics of the atmosphere. In this category are found a number of possible mechanisms: (a) the feedback of high-frequency eddies onto the low-frequency components of the flow (Lau and Nath 1991; Cai and Van den Dool 1991), (b) so-called weather regimes, in which high- and low-frequency variability equilibrate (Reinhold and Pierrehumbert 1982), (c) the existence of nearly steady states (Branstator and Opsteegh 1989; Anderson 1992) including modons and blocked flow, (d) barotropic instability of the time-mean flow (Simmons et al. 1983; Anderson 1991), which could be determined indirectly by the geographically fixed features of the earth (e.g., land–ocean interface, terrain), (e) midlatitude connections to the tropical Madden–Julian wave (Madden and Julian 1971), (f) traveling free Rossby waves (Lanzante 1990 and references therein), and (g) traveling "modes" as revealed by an empirical orthogonal function (EOF) analysis (Branstator 1987). The seven mechanisms in the second category could operate without any anomalous external forcing. They are intertwined in many ways and it is difficult to rank them in terms of importance. In most circumstances the second category appears to dominate the first in midlatitudes. There are also combined internal dynamics/external forcing proposed mechanisms. One example is a zonal index cycle–like phenomenon (Jin and Ghil 1990; Bernardet et al. 1990) in which the mountain drag on the midlatitude westerlies causes quasi-periodic momentum exchanges with the solid earth with a time scale of 20–70 days.

The compiling of standard deviation statistics in an atlas and some discussion of the major features therein in this paper is intended to increase our understanding of these physical processes in addition to providing reference material for more descriptive purposes and for forecast applications.

2. Data

The data consist of monthly mean 700-mb height at 358 grid points from 15° to 90°N, derived from twice-daily data from 1950 through 1991 from NMC. Each of the 15 5-degree-apart latitude circles contains 36 grid points with longitudes offset by 5° on successive latitude circles such that a diamond configuration is created. Fewer points are included at higher latitudes to establish an approximate equal area representation. Further details on this grid and on the treatment of brief missing periods in the early part of the record and an early 1950s positive bias are described in Barnston and Livezey (1987). Because the 15°N latitude circle and an area in the low-latitude eastern hemisphere contain the most noticeable missing data problem, points in these locations were omitted from the analysis.

3. The mean state

In order to more fully appreciate the interannual variability, it is desirable first to note the mean height relative to which the standard deviation is computed. The mean 700-mb height in the extratropical Northern Hemisphere for the 1950–91 period is shown in Fig. 1 for the months of January (a), April (b), July (c), and October (d). Departures from the zonal-mean flow (termed "eddy") in these four portions of the annual cycle are shown in parts (e), (f), (g), and (h). In most regions of the hemisphere there is a gradual amplitude increase from summer to winter. The general similarity of the phasing of these fields in North America over the annual cycle reflects, in our view, their association with geographically fixed features such as terrain, oceans, etc. On the other hand, there is an annual oscillation in the sign of the eddy component in central and southern Asia versus the Pacific, in which the relatively warmer surface is associated with lower heights

[as found more pervasively for sea level pressure (Hsu and Wallace 1976) and surface pressure (Van den Dool and Saha 1993)].

4. Interannual variability

The interannual variability is described using the standard deviation of the monthly mean 700-mb height over the 42-year period of record, by individual grid point, for three pooled adjacent months centered on any given month of the year. Pooling is carried out to reduce sampling uncertainty, which will be discussed further below in the context of the trustworthiness of suggested seasonal changes. In the pooling process the standard deviations are computed using squared deviations with respect to the mean of the appropriate individual month. The resulting standard deviation fields representing each of the four regular seasons (winter consisting of December, January, and February, etc.) are displayed in geopotential meters (gpm) in Fig. 2. Inspection of these fields shows increases in variability with latitude up to about 45° to 50° at all times of the year, northward of which the variability depends more on longitude than latitude because several focal points of maximum variability are found in this general latitude region. In sections 4a and 4b, we discuss the high- and low-variability regions, respectively.

a. Peak variability regions

There appear three rather stable year-round sites of peak variability at latitude 45°N and higher that we wish to explore in somewhat more detail. While referring to them as peak variability regions, we notice that by considering the outermost closed contour, each of these areas tend to cover 25° latitude by 70° longitude—that is, roughly half of the high-latitude ocean basins.

In all 12 months there is a peak in variability in the northern Pacific Ocean, near or slightly south of the western end of the Aleutian Islands. This site exhibits smaller month-to-month locational fluctuations than the other two, although it is not always the strongest of the three. The second most reliable location to find a peak in variability is in the northern Atlantic Ocean, south of Iceland and west of the British Isles. A third preferred region, with some relatively marked month-to-month meanderings, ranges from east of Scandinavia or near Novaya Zemlya to the Taymyr Peninsula or the North Pole. We will refer to these three peaks as the Pacific, Atlantic, and Arctic peaks, respectively. These peaks also appear in Blackmon et al. (1984) using 500-mb height data for winter. Their standard deviation field for 30-day means (see their Fig. 2b) closely resembles Fig. 2a here, even though intraseasonal fluctuations are included in their field but not in ours. Roughly similar patterns are also found in Blackmon et al. (1984) even when a variety of other filtering schemes is used.

The month-to-month positions of the variability peaks for each of the three peak regions are displayed in Fig. 3, based on individual (unpooled) one-month standard deviation fields (not shown here, but winter months included in Barnston and Van den Dool 1993). In Fig. 3 the month number labels are defined with 1 = January, 9 = September, A = October, and C = December. Labels in parentheses indicate secondary locations within the same region (peaks of lower magnitude) in addition to the primary one. All three regions are represented in all 12 months, although there are sometimes relatively weaker signatures. It is clear that the Pacific maximum is contained in a remarkably small area (given the large changes in flow from summer to winter) while the other two areas are larger, reflecting greater month-to-month changes in the location of peak variability. In most seasons the Arctic and Atlantic maxima appear to be part of a bigger complex area of high standard deviation.

One might reasonably question whether the changes in location of maximum variability are physically real or only a reflection of sampling variability. We remind the reader that 42 years is not a large sample for the estimation of second or higher moments. In attempting to resolve this issue it is helpful to estimate quantitatively the sampling variability of a sample standard deviation based on N independent realizations of a variable. Assuming that a variable is normally distributed, a confidence interval with a probability-prescribed width for the variance of the variable is given by the appropriate upper and lower cutoff values of the chi-square distribution with $N - 1$ degrees of freedom (Hays 1973). In particular, the confidence interval for the population variance is given by $(N - 1)s^2/X^2$ where s is the sample standard deviation and X^2 is the value of chi square at the appropriate lower and upper cutoff points on its distribution for $N - 1$ degrees of freedom. For significance level p, the $100(1 - p)$ percent confidence interval would be formed using the X^2 values at the $p/2$ and $1 - (p/2)$ cutoff points for the lower and upper limits of the interval, respectively. The square roots of these variance limits give the standard deviation confidence interval.

Applying these principles to unpooled 42-element sample standard deviations used in Fig. 3 and elsewhere in this paper (assuming normality and negligible interannual autocorrelation in the 700-mb heights), the 95 percent confidence interval is found to span from $0.82s$ to $1.28s$, where s is the sample standard deviation. This wide interval serves as a warning that the standard deviation is considerably vulnerable to sampling variability, requiring more caution in interpreting changes than would be needed for an entirely linearly computed parameter such as the mean. The month-to-month differences in standard deviation involved in many of the peak variability location changes shown in Fig. 3 do

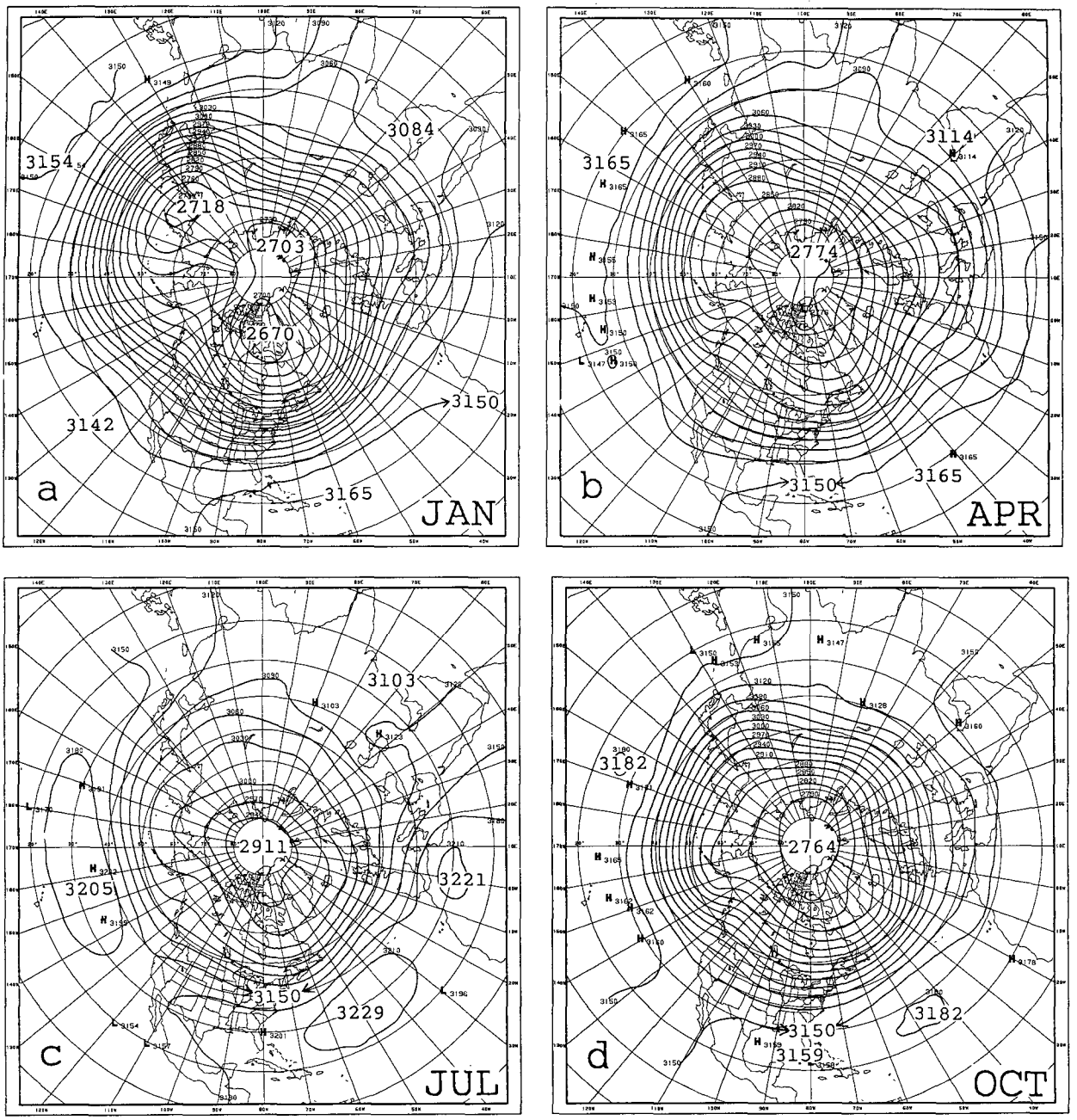

FIG. 1. The monthly mean 700-mb height in the extratropical Northern Hemisphere over the 1950–91 period for (a) January, (b) April, (c) July, and (d) October; contour interval 30 gpm. Parts (e), (f), (g), and (h) are the eddy component of the January, April, July, and

not fall outside this confidence interval. Greater credibility can be found, however, when the seasonal locational shifts exhibit continuity among groups of consecutive months (e.g., at least two, and preferably more) as in an intraannual oscillation. When three months of data are pooled in evaluating the standard deviation of the central month as in Fig. 2, the 95 percent confidence interval narrows to $0.89s$ to $1.14s$, allowing smaller case-to-case differences to be regarded as physically meaningful.

Using the above caveat in interpreting Fig. 3, some seasonality can be identified. During the three summer months the Arctic variability peak principally relocates to the Alaskan side of the North Pole, with a comparatively weak residue in the "normal" position, and during midfall to early winter there is a marked mi-

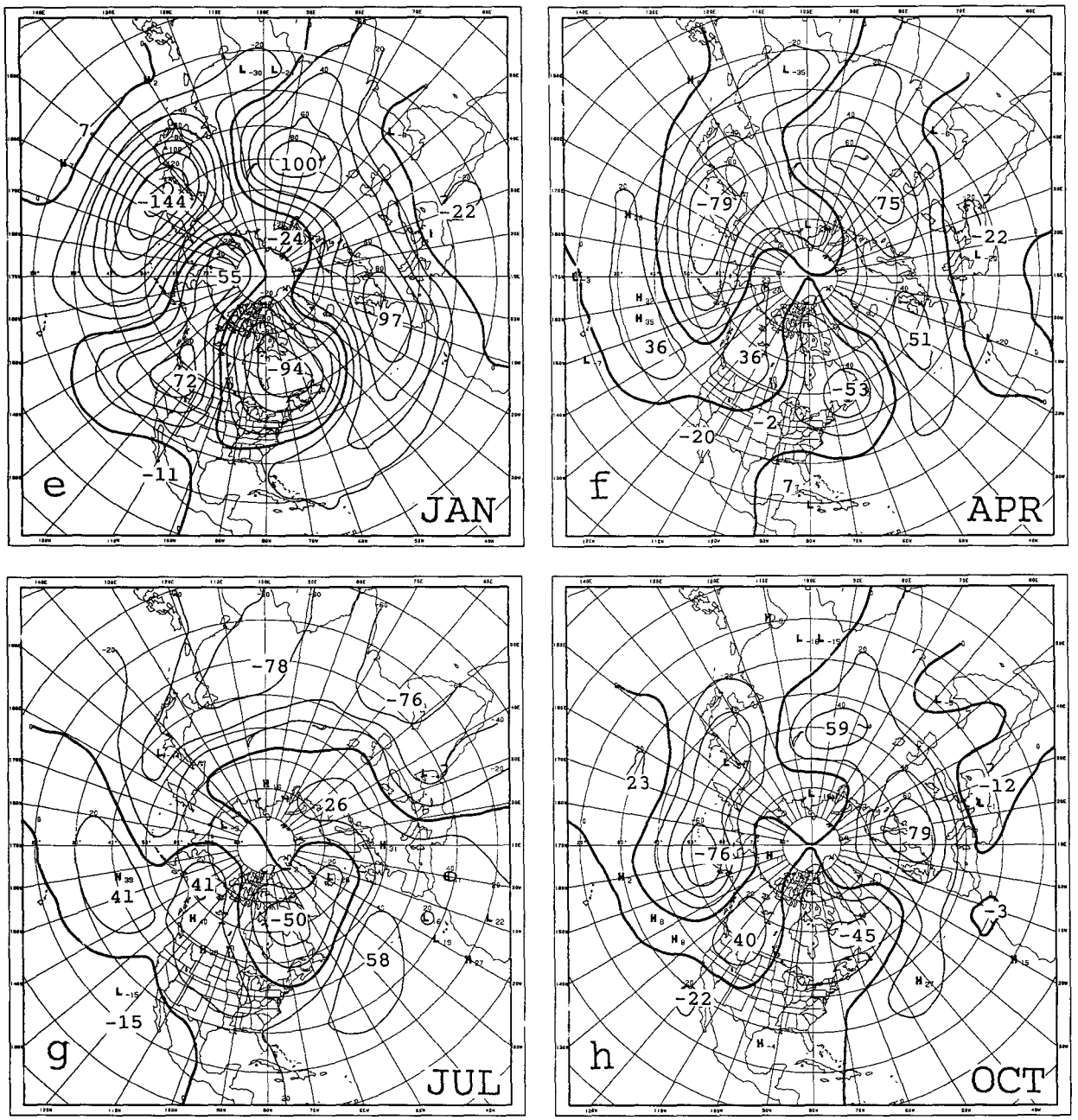

FIG. 1. (*Continued*) October height fields, respectively, where the zonal mean at each latitude has been removed; contour interval 20 gpm.

gration southwest into the Eurasian continent (this being the only time there is a standard deviation maximum over land). Seasonality in the Pacific peak is less certain (but remarkably small in any case), with a tendency to be positioned farther east in late summer/early fall and farther west in middle to late spring. The Atlantic peak is more locationally stable than the Arctic peak but less so than the Pacific peak. There is a tendency for a westward migration of this peak from midwinter through early spring (with marked excursions in January and March) although a weaker residue appears in the "normal" position in these cases.

Except for the summer migration of the Arctic variability peak across the North Pole, there is, surprisingly, no general tendency for the peaks to move northward with the approach of the warm season and southward again in fall despite the fact that 1) the jet stream displays such seasonal pulsation (Figs. 1a,b) and 2) the cyclone tracks move north and south with season (Klein 1957; Byers 1974; Wallace 1987, and references

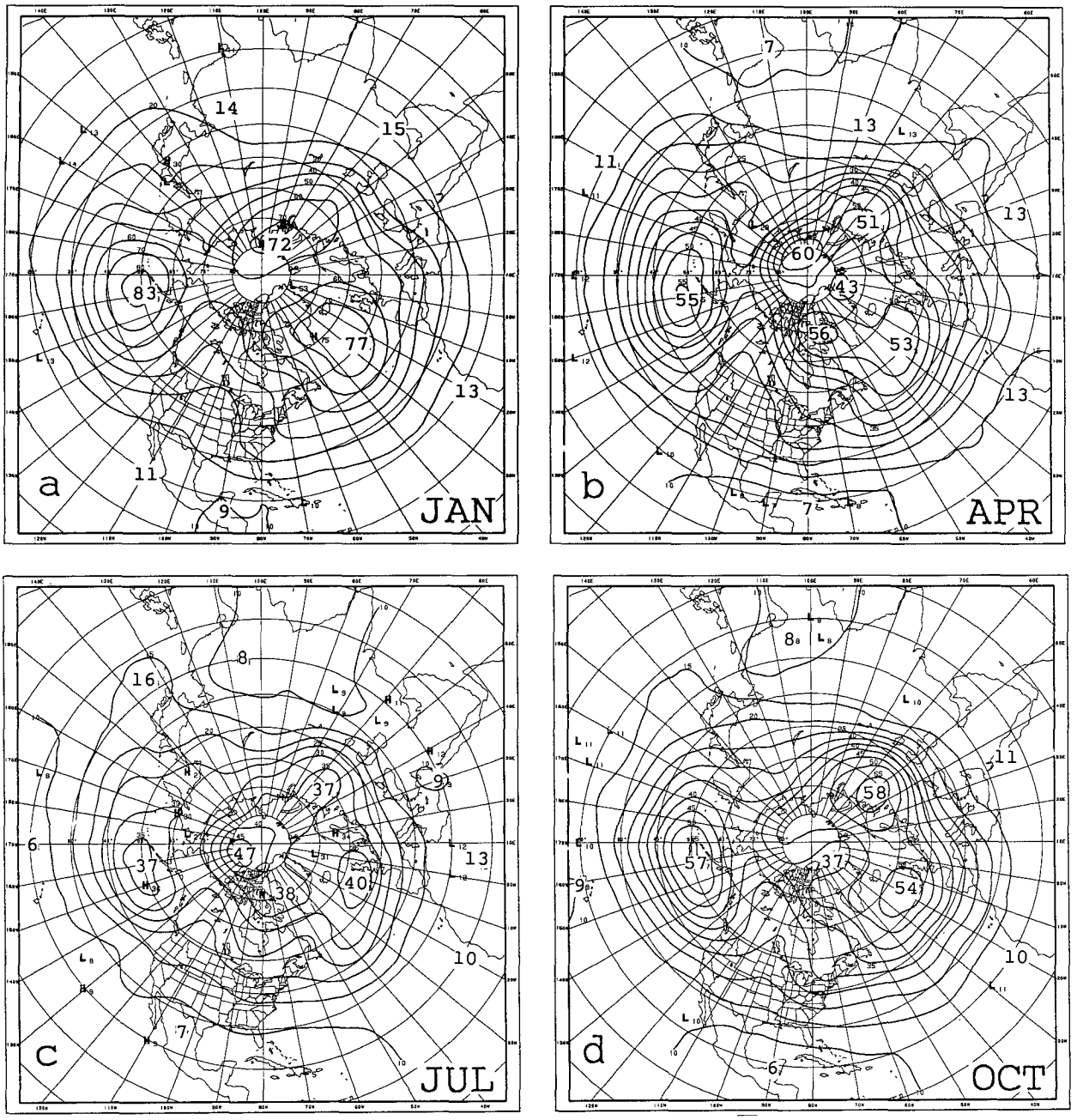

FIG. 2. Geographic distribution of the interannual standard deviation of monthly mean 700-mb height for the 1950–91 period for (a) January, (b) April, (c) July, and (d) October in the extratropical Northern Hemisphere. A pooling of the standard deviation over the three-month period centered at the target month has been done to reduce sampling variability. Contour interval is 10 gpm for January, 5 gpm otherwise.

therein). This oscillation in the jet stream occurs largely to the south of the peak variability areas (i.e., 35° to 50°N in summer versus 25° to 45°N in winter).

Figure 4a shows the peak one-month mean standard deviation values in each of the three high-variability regions as a function of month for unpooled data. The regions have approximately a two-to-one winter-to-summer peak variability ratio, with standard deviations ranging from 80 to 95 gpm in winter and 35 to 50 gpm in summer. The Pacific region (solid line) shows the most seasonality and the Arctic region (line with larger dashes) the least. When the standard deviations are computed pooling three adjacent months' data, the month-to-month variations of peak values in the three

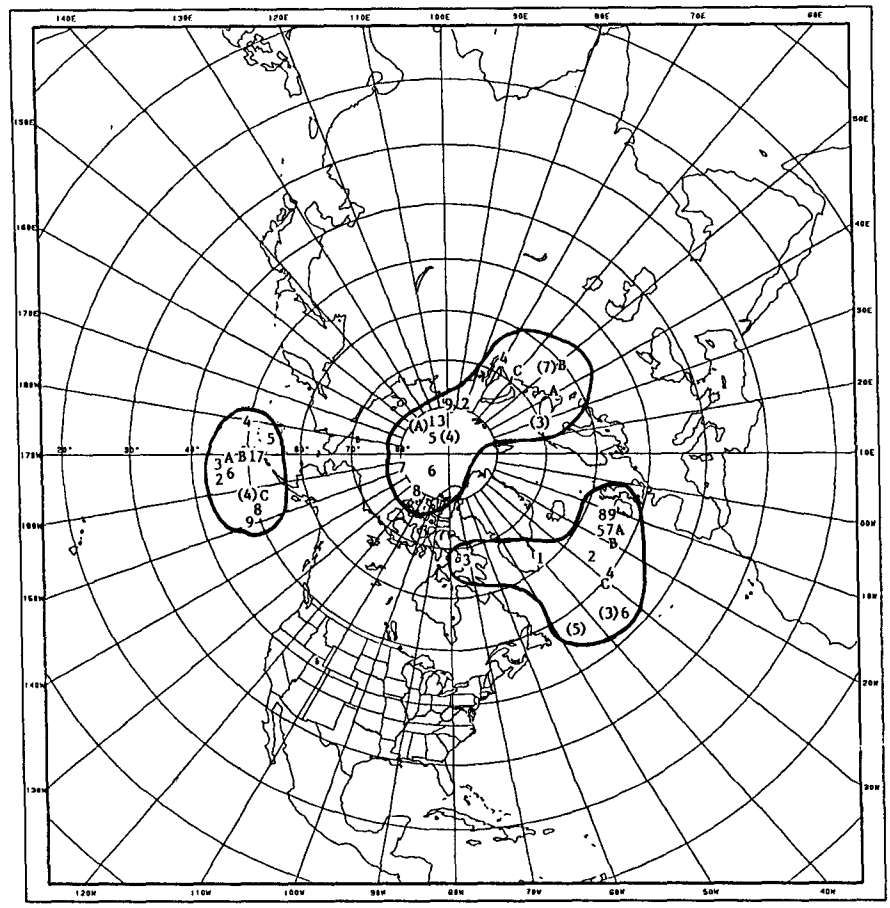

FIG. 3. Locations of the 12 one-month (without pooling) standard deviation maxima by month number for the three general peak regions discussed in the text (1 = January, 9 = September, A = October, C = December). Secondary maxima for a given month and region are indicated by parentheses.

regions (Fig. 4b) are reduced from those of Fig. 4a because the pooling process "trims away" the details of the standard deviation field. This is a reasonable expectation in light of the month-to-month locational shifts in peak variability. The pooled results suggest no marked differences in peak value behavior among the three high-variability regions, with summer values roughly 35–50 gpm and winter values roughly 80–90 gpm.

Figure 5 presents the maximum, mean, and minimum values of the one-month standard deviation over the entire Northern Hemisphere grid (from 20° northward)—for unpooled data in part (a) and three-month pooled data in (b). (The mean is computed as the square root of the average of the gridpoint variances.) The maximum value always equals that of one of the peak variability regions as shown in Fig. 4. The minimum hemispheric variability values, occurring just outside the tropics, have a seasonality phased similarly to that of the rest of the hemisphere within their range of 6 to 10 gpm. Figures 4 and 5 show that the seasonal variation in the high-variability regions, to first order, is proportional to the seasonal variation in standard deviation of the hemisphere as a whole, that is, highest (lowest) standard deviation occurring in January/February (July).

Figure 6 is a plot of the year-to-year time series of the one-month mean (unpooled) height at 50°N, 170°W (near the center of the Pacific peak variability region) for January and July. The high variability of the height at this location is evident, with some of the adjacent-year January fluctuations nearly as great as the mean difference between January and July. Even in July the range in monthly mean values is greater than 150 gpm. Because this location is close to a center of the winter Pacific/North American (PNA) pattern (Wallace and Gutzler 1981; Horel 1981; Esbensen 1984; Barnston and Livezey 1987), the January fluctuations are strongly related to fluctuations of the amplitude of the PNA. A discontinuity marking a large interdecadal variation in the January height between 1950–75 and 1976–92 is strongly suggested with heights

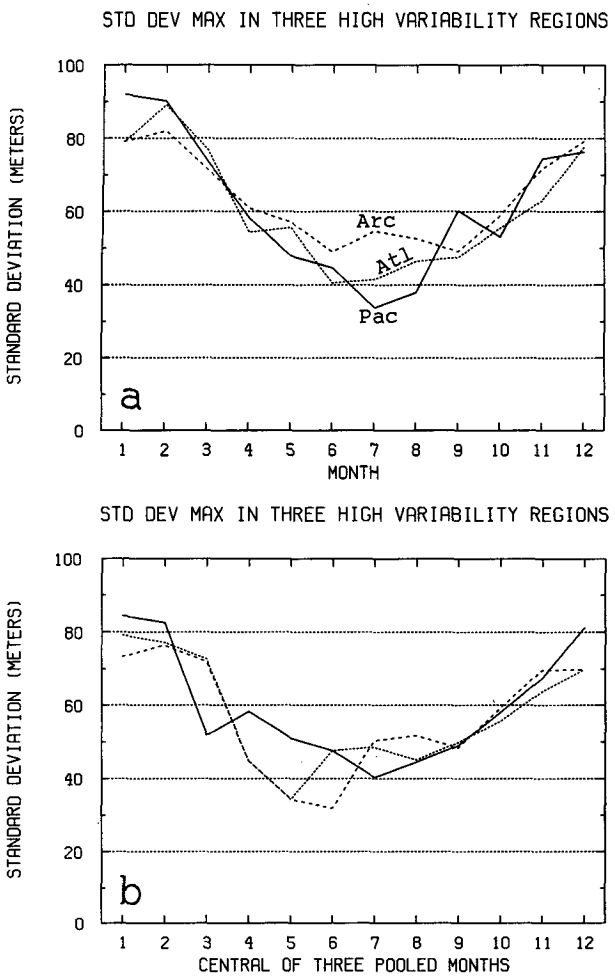

FIG. 4. Value of peak one-month mean standard deviation of 700-mb height (gpm) in each of the three high-variability areas as a function of month, for (a) unpooled standard deviations and (b) pooled standard deviations using three consecutive months of data. Values for the Pacific area are shown by the solid line, the Atlantic area by the short-dashed line, and Arctic area by the long-dashed line.

in the latter period averaging almost 100 gpm lower than those in the earlier period. This coincides with a similar trend in cold season sea level pressure (Douglas et al. 1982) and SST (Trenberth 1990) in a broad region in the North Pacific, and an increase in the observed frequency of winter occurrence of the positive phase of the PNA pattern over the last 15 years among operational long-range forecasters at CAC. Interdecadal variability clearly contributes a portion of January's interannual standard deviation in the Pacific maximum variability region. At 50°N, 170°W (Fig. 6), for example, the least-squares linear trend line (which runs from 2857 m in 1950 to 2737 m in 1991) contributes nine percent of January's standard deviation (17 percent of the variance). The standard deviation at the Atlantic peak variability site also, to a lesser extent, is enhanced in winter by interdecadal variability (not shown), in the form of a greater frequency of occurrence in recent years of the North Atlantic Oscillation (NAO) with a negative anomaly center over southern Greenland. However, long-term trends or interdecadal variability of the magnitude shown in Fig. 6 do not, in general, contribute strongly to any of the three variability peaks for more than a small portion of the year.

The month-to-month changes in location (Fig. 3) suggest sampling variability in the 42-year analysis period. To determine whether one or two outliers in the time series for a given month can substantially affect the resulting standard deviation, histograms of monthly mean 700-mb height at relevant individual grid points were examined. The findings are that conspicuous outliers do occur, and are responsible for many of the location and intensity variations of the one-month unpooled standard deviation peaks. For example, there is an increase in the intensity of the Atlantic variability

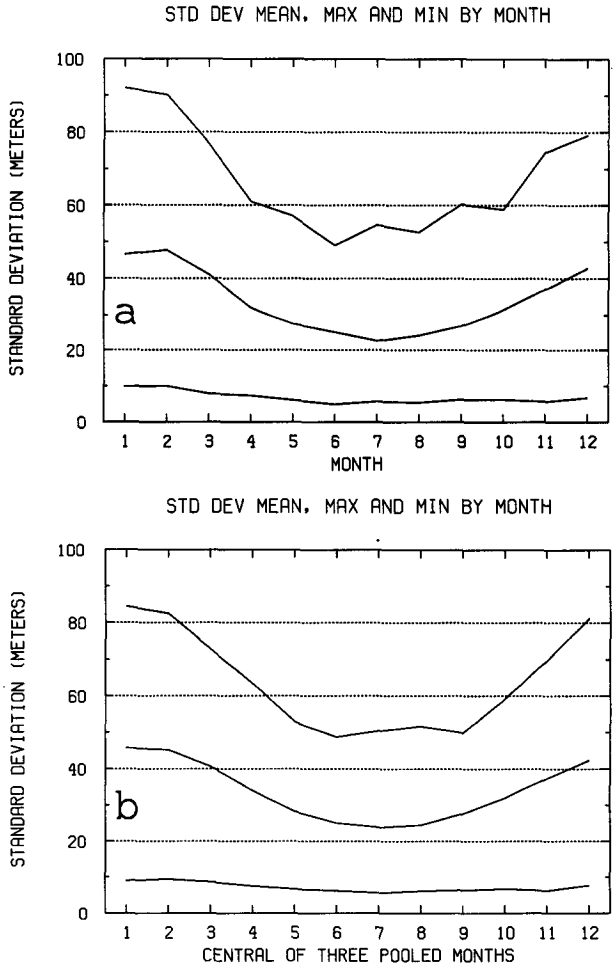

FIG. 5. Maximum, mean, and minimum of the 358 gridded values of one-month-mean 700-mb height standard deviation in a single monthly mean map (gpm) as a function of month, for (a) unpooled standard deviations and (b) pooled standard deviations using three consecutive months of data.

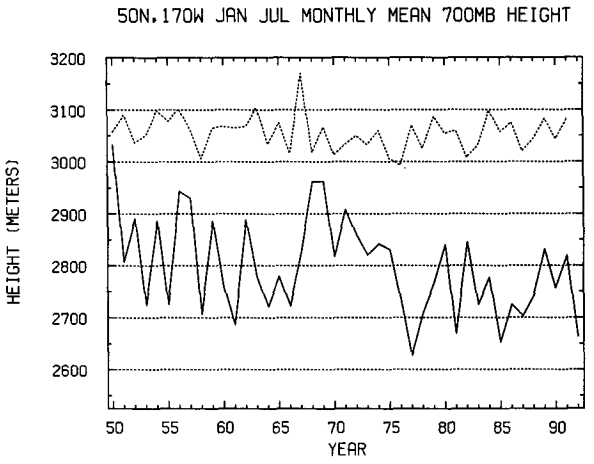

FIG. 6. Time series of January (solid) and July (dashed) monthly mean 700-mb height (gpm) over the 42-year study period at 50°N, 170°W at the Pacific high-variability site. No pooling of data has been carried out.

peak from 78 to 88 gpm from January to February (see Fig. 4a). Table 1 represents a histogram of the monthly mean heights at the grid point at 60°N, 25°W (near the center of the Atlantic variability peak) in January and February. In January both an outlier low height of 2612 gpm (in year 1974) and a blocking-related outlier high height of 2994 gpm (1963) occurred relative to the mean of 2801 gpm. In February a still more extreme set of outliers took place with a low of 2605 gpm (1990) and a dramatically higher high of 3068 gpm (1965) compared with a mean of 2824 gpm. The February 1965 height anomaly at this location is among the highest ever observed anywhere in the hemisphere in the 1950–91 period [being surpassed in magnitude only slightly by the positive anomalies at 60°N, 150°W in February 1989 and at 55°N, 165°W in January 1950; note that both of these are located near the Pacific peak variability site during negative (cold) ENSO episodes]. The February 1965 height exceeded that of the year having second highest height by over 100 gpm, with clear-cut implications for the standard deviation parameter. In fact, it is found to increase the interannual standard deviation by 11 percent (and the mean by 6 gpm), its own standardized anomaly value being 3.00 when 1965 is included in the distribution and 3.43 when not included. The standardized anomalies are even greater when the outlier height anomaly does not occur at the point of maximum variability, as was the case in February 1989 at 60°N, 150°W which was approximately four standard deviations above the mean.

b. Minimum variability regions

In addition to the variability peaks, Fig. 2 shows regions of minimum standard deviation other than those accompanying low latitudes in all seasons. Unlike the variability peaks, the lows tend to appear as unclosed elongated "troughs" (although we will refrain from using that term) with defined axes. Minima in variability may be found in west-central North America in nearly all individual months (shown for winter months in Barnston and Van den Dool 1993) as well as in the seasonally pooled one-month standard deviations in Fig. 2. While minima may also occur in the east-central former Soviet Union or near Scandinavia, they are less pronounced and harder to track over the annual course.

Figure 7 shows the locations of minima in the unpooled monthly standard deviation fields (not shown)—that is, areas of local minimum variability. In most months a clearly delineated south-southeast to north-northwest North American axis of minimum variability appears with the southern end in the central United States or south-central Canada and the northern end often in northeastern Alaska or adjacent northwestern Canada. This is undoubtedly related to the orography. Here the standard deviation can be as low as 20 gpm throughout much of the year. Exceptions to this are found only in January (in which only a weak version of this phenom-

TABLE 1. Histogram table of frequency of occurrence of monthly mean heights at 60°N, 25°W (south of Iceland) in 20-m intervals for the 42 years of January and February, 1950–1991.

700-mb height interval (m)	Frequency Jan.	Feb.
3080–3100		
3060–3080		1
3040–3060		
3020–3040		
3000–3020		
2980–3000	1	
2960–2980		
2940–2960		2
2920–2940		3
2900–2920	1	1
2880–2900	4	2
2860–2880	4	4
2840–2860	5	2
2820–2840	2	5
2800–2820	3	8
2780–2800	2	1
2760–2780	8	5
2740–2760	4	4
2720–2740	3	
2700–2720	3	1
2680–2700		2
2660–2680	1	
2640–2660		
2620–2640		
2600–2620	1	1
2580–2600		
2560–2580		
2540–2560		
2520–2540		

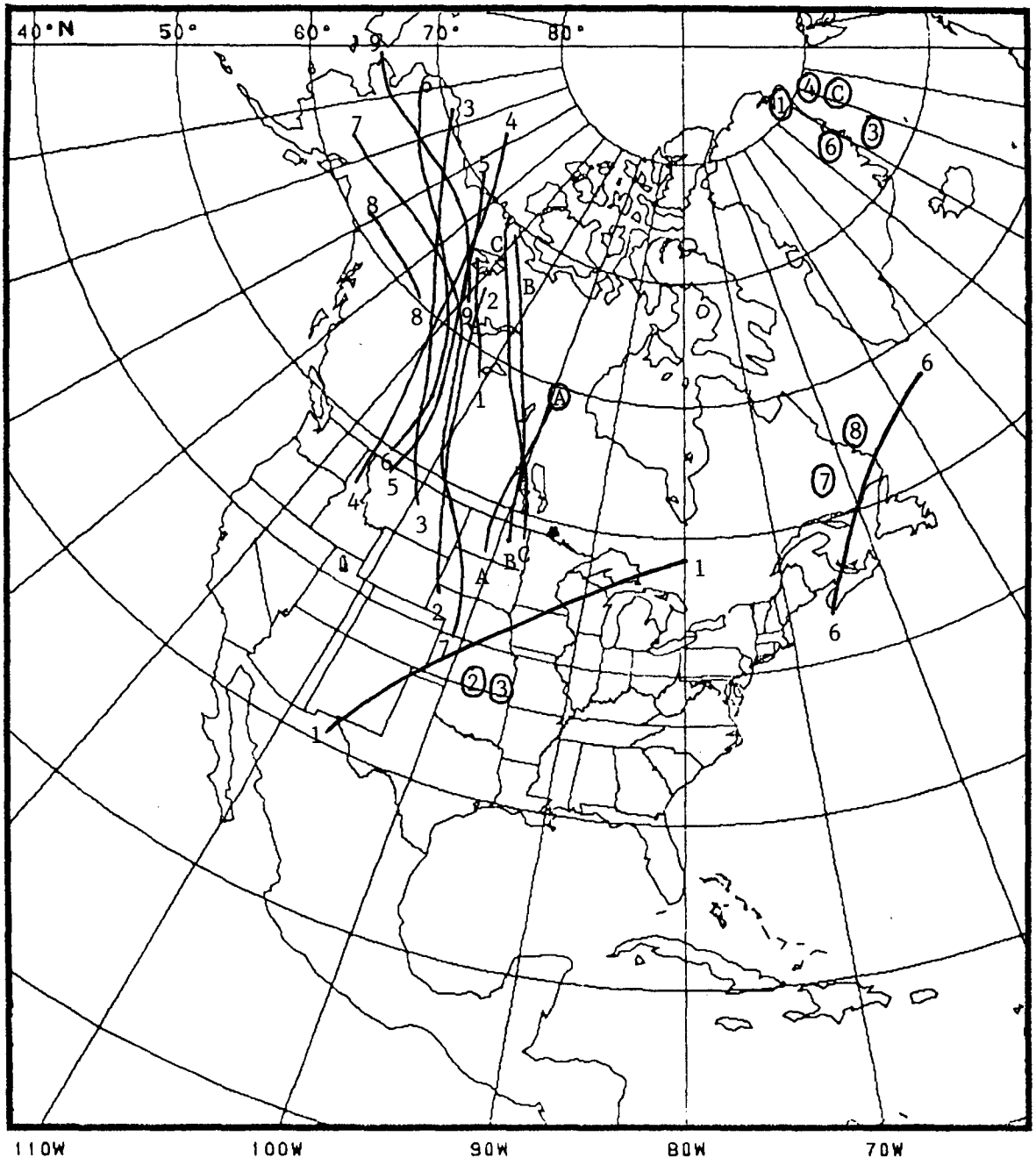

FIG. 7. Standard deviation minimum axes by month number (without pooling; same labeling system as in Fig. 3). Minimum points are also indicated when present.

enon occurs, with a stronger minimum variability axis running nearly perpendicularly from the southern U.S. Rockies to eastern Canada) and August (marked by a relative absence of a minimum). In March and April variability minima are found east of upper Greenland.

Regions of low variability are important because, among other things, they are favorable sites in which to examine phenomena of the very lowest frequency such as climate change, changes in observation or analysis methods, etc. These sites have minimal natural variability to obscure subtle underlying "signals" that would otherwise require longer periods of record to identify.

Figure 8 is a plot of the year-to-year time series of the one-month mean (unpooled) height at 50°N,

110°W (just north of the state of Montana in the United States, in the major low-variability region) for January and July (part a), April and October (part b), and for the cold half (November through April), warm half (May through October), and all of the year (part c). The relative lack of variability here is evident in comparison with Fig. 6 for January and July, even though the January minimum in variability (shown in Fig. 7) does not occur precisely at the location used for Fig. 8. The time series for the average of the six coldest, six warmest, and all 12 months (Fig. 8c) is remarkably noise free, showing some peculiar-looking fluctuations that apparently penetrate both halves of the year (note the high values for 1952, 1987; the low values for 1964 and especially 1975). The presence of these relative extreme points, of unknown cause, would go unnoticed at "noisier" locations whose height is forced by a multitude of mechanisms. A general trend over time is not evident in Fig. 8, nor are there obvious discontinuities that could be caused by changes in instrumentation or analysis techniques. The idea of the North American low-variability region being along the node of spatially coherent variability patterns will be explored further in the next section.

5. Variability peaks as anomaly centers and members of multicenter patterns

One might ask whether the variability peaks described in section 3 represent the centers of frequently occurring anomaly patterns, and the variability minima a relative absence of occurrences of such centers. An alternate possibility is that the standard deviation minima may occur where there are centers also, but of weak anomaly magnitude. A second question is whether or not the variability peaks are related to the centers of the preferred patterns found in teleconnection studies (Namias 1981; Wallace and Gutzler 1981; Esbensen 1984) or principal components analyses (PCA) (Horel 1981; Barnston and Livezey 1987). This possibility has already been raised by noting the locational congruence of the Pacific variability peak with a major center of the PNA pattern.

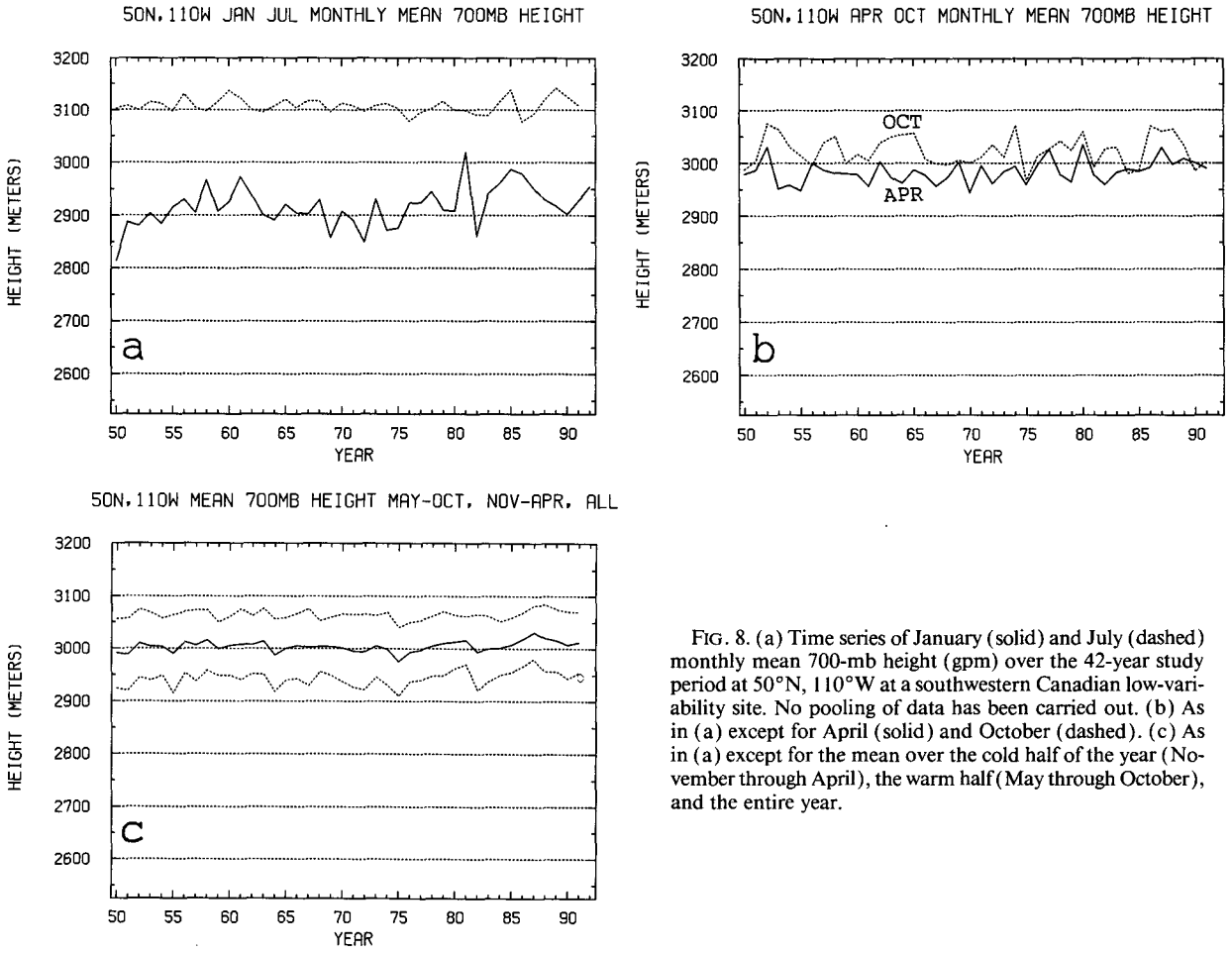

FIG. 8. (a) Time series of January (solid) and July (dashed) monthly mean 700-mb height (gpm) over the 42-year study period at 50°N, 110°W at a southwestern Canadian low-variability site. No pooling of data has been carried out. (b) As in (a) except for April (solid) and October (dashed). (c) As in (a) except for the mean over the cold half of the year (November through April), the warm half (May through October), and the entire year.

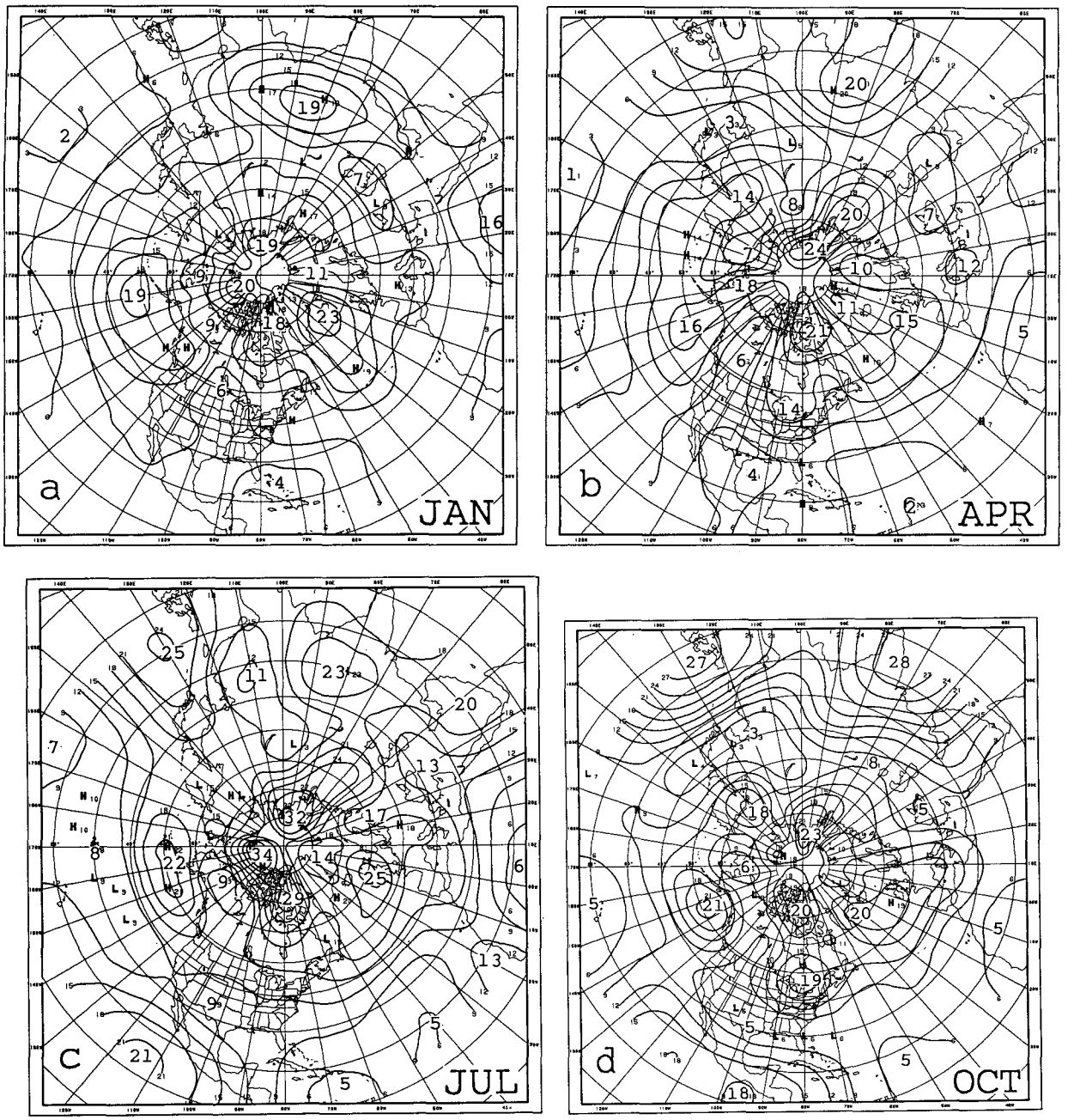

FIG. 9. Geographical distribution of frequency of occurrence (×10) of positive or negative monthly mean 700-mb height anomaly centers in (a) December, January, and February, (b) March, April, and May, (c) June, July, and August, and (d) September, October, and November. Contour interval 3.

a. As anomaly centers

To help determine the answer to the first question, frequency counts for spatial maxima and minima were conducted to obtain a field of frequency of occurrence of anomaly centers. There is a choice regarding what should be counted as an anomaly center. At the lenient end of the spectrum, a location having an anomaly of either sign would qualify as long as none of the surrounding points (within a radius appropriate for the spatial scale) have larger anomalies of the same sign. This "easy" rule was used in the seminal work by O'Connor (1969) in qualifying cases to be used as base points for sign-specific teleconnections. A continuum of stricter options would be to require the above, but also require that the anomaly in question have a value

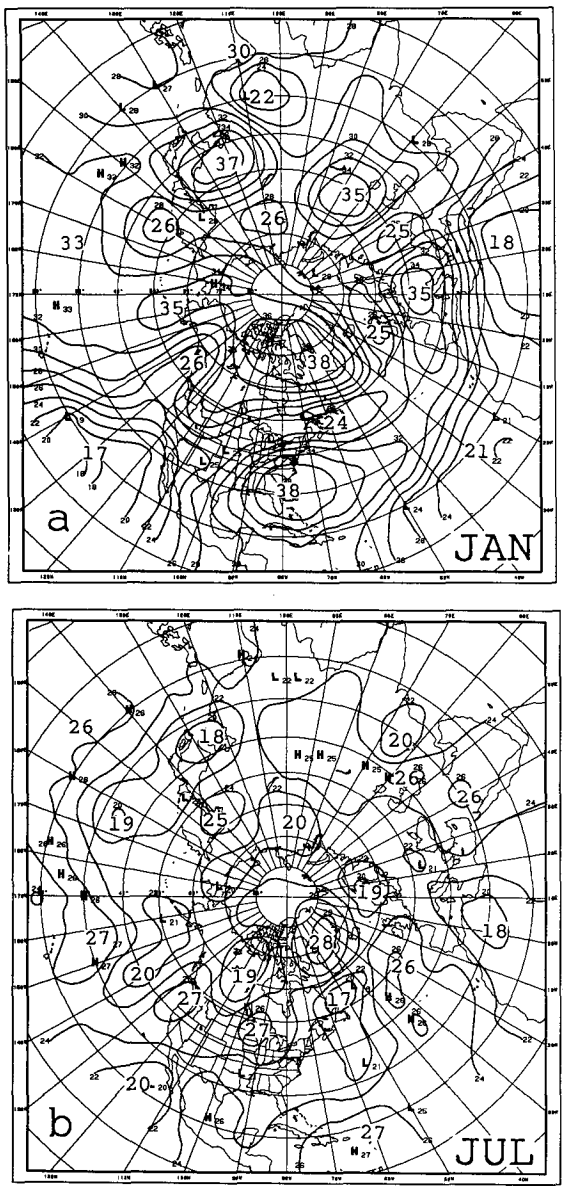

FIG. 10. Field of total teleconnectivity based on 1950–91 monthly mean 700-mb height data for (a) January and (b) July, computed as the mean correlation (multiplied by 100) between each base grid point and all other grid points. The individual correlation coefficients are squared and then averaged, and the result is square rooted. Contour interval 2.

exceeding a threshold. The stricter options reject weaker cases in hopes of increasing the signal to noise ratio, but risk leaving too small a sample. This type of selection criterion was used by Wagner and Maisel (1988) for qualifying cases to update the O'Connor (1969) work. In the present study a moderately strict criterion was chosen: to be tallied as a center, the height at a given grid point must be at least one standard deviation away from its mean and must be surrounded by height values of lower anomaly magnitude at the six surrounding grid points. The frequencies are derived from a 541-point quasi-regular latitude–longitude grid, but are normalized for differing areal representation so that the counts reflect frequencies of extrema for 10° longitude intervals at 60°N. The monthly mean height patterns of three adjacent months were pooled to reduce sampling uncertainty, and the resulting frequency field was then smoothed spatially with three passes using a binomial weighting scheme and the same radius as that used for the identification of extrema. Figure 9 shows the frequency fields, multiplied by 10, for winter (December, January, February), spring, summer, and fall. A relationship between the variability peaks in the seasonally pooled maps shown in Fig. 2 and the highs in the frequency counts of the corresponding seasons in Fig. 9 is clearly visible. (An exception occurs in Tibet in January and July.) The relationship holds in analogous fashion for the west central North American variability minimum region in all seasons—low standard deviation values coincide with low frequencies of occurrence of extrema.

The variability minimum region can be viewed as a node between height anomaly centers on either side. To confirm this notion with greater certainty, the anomaly patterns accompanying occurrences of the highest-magnitude standardized anomalies at variability minimum points such as 45°N, 105°W (eastern Montana/Wyoming border) were inspected. In all of the cases inspected, the nearest anomaly center is located somewhat far from the minimum region (e.g., near the Pacific coast or in the eastern half of Canada or the United States), with the minimum point participating only peripherally in terms of its departure from normal (in gpm) but more heavily as a standardized anomaly.

b. As members of multicenter patterns

The question regarding the participation of the peak variability centers in coherent multicenter anomaly patterns can be addressed in a number of ways. The field of mean teleconnectivity can be computed to determine the general communality, or connectedness, of the heights at each location with all other locations collectively. Principal components (PC) analysis can also be used to help identify spatially coherent portions of the gridwide variability, and perhaps reveal more specifically how the variability at one or more of the three peak variability sites is related to the variability elsewhere.

1) FIELD OF MEAN TELECONNECTIVITY

The quickest approach to evaluating the total participation in systematic patterns on the part of each

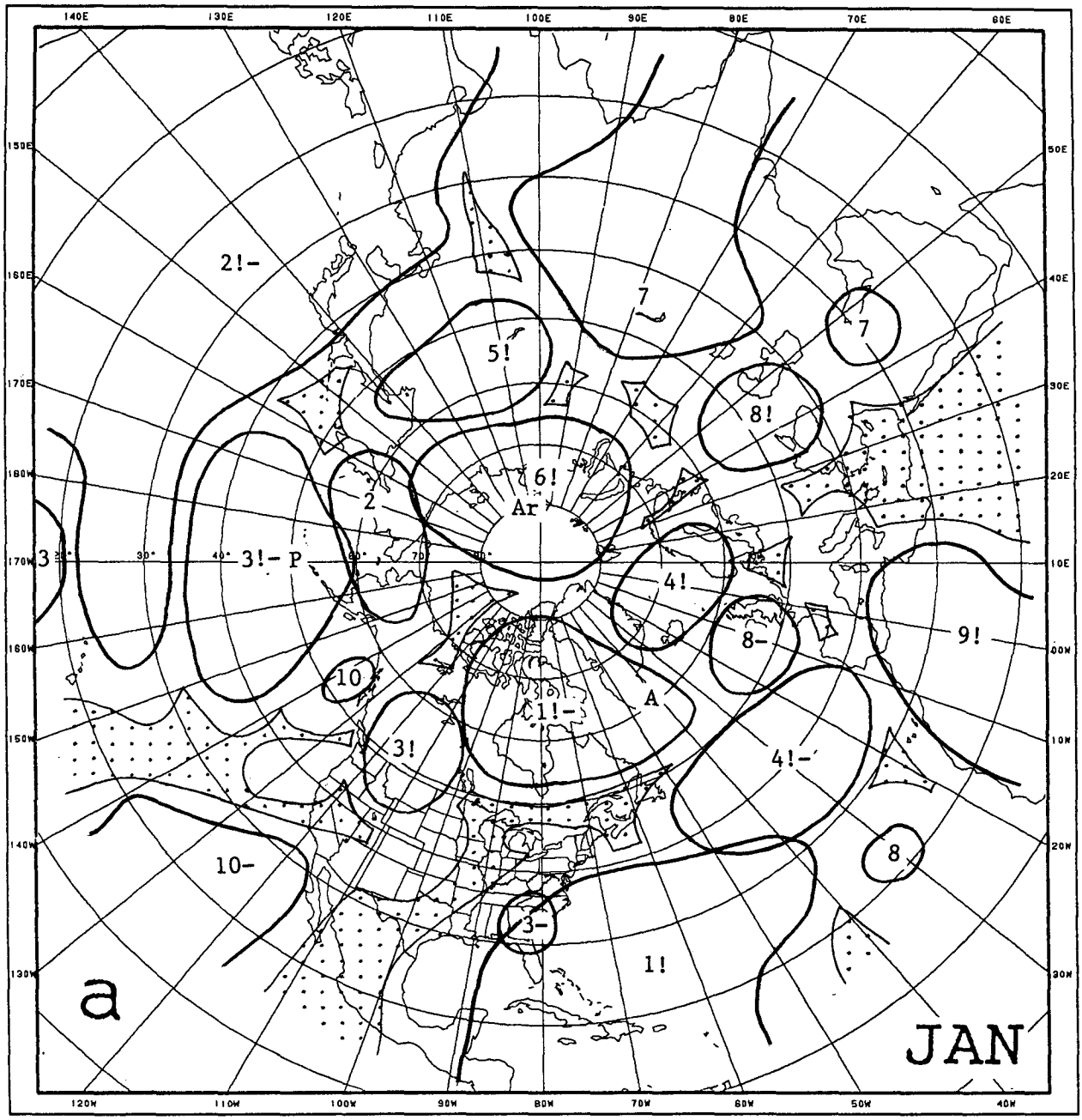

FIG. 11. The rotated PC spatial loading patterns of the leading 10 modes of individual monthly mean 700-mb geopotential height over the 1950–91 period for (a) January and (b) July. Patterns are outlined using as threshold the 0.6 correlation between the principal component time series and the original gridpoint data. Mode numbers are shown at position of maximum loading magnitude; exclamation point

high standard deviation site is to compute each of the 358 grid point's mean teleconnectivity (Wallace and Gutzler 1981), or covariability with respect to all other grid points, and note whether the three sites rate highly relative to other locations. Resulting mean teleconnectivity fields for January and July are shown in Fig. 10, based on the 1950–91 period of monthly mean 700-mb height data. Mean teleconnectivity is computed as the mean correlation between a base grid point and all other grid points, where the 357 correlation coefficients are squared, averaged, and the result square rooted. The maxima in the average

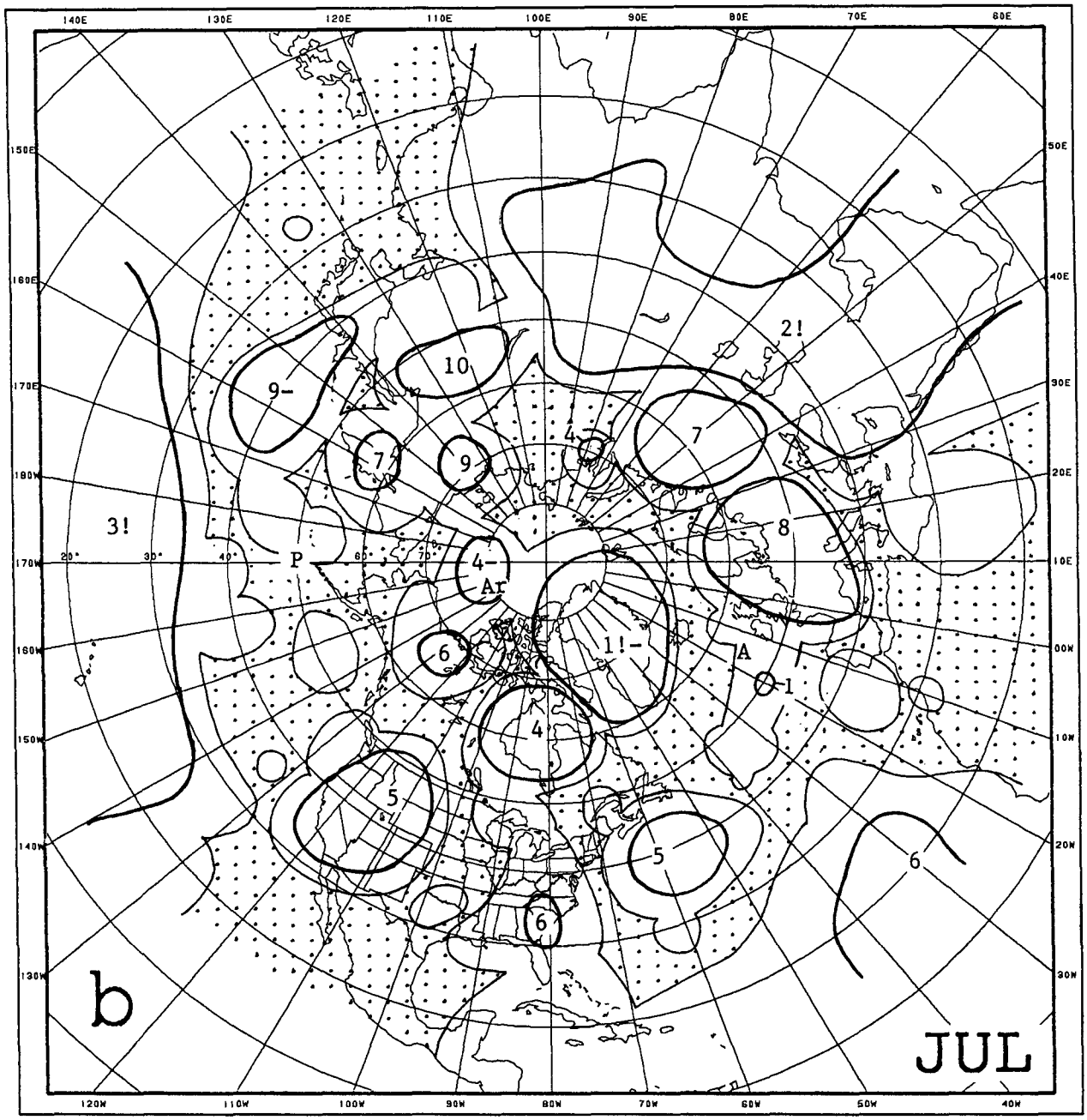

FIG. 11. (*Continued*) indicates magnitude of 0.8 or greater. Minus signs denote relative polarity among centers of multicenter patterns. The stippled areas have no 0.45 or greater magnitude of loadings among the leading 10 modes. The locations of the three sites of maximum standard deviation are marked with A (Atlantic), P (Pacific), Ar (Arctic).

teleconnectivity fields do not generally indicate a preference for the three high-variability sites in January or July. Only the Pacific site in January and the Atlantic site in July appear well connected. The mean teleconnectivity field shows greater seasonal dependence than the standard deviation field. High interannual variability does not appear to be closely linked with total participation in spatially coherent variability patterns.

2) PC ANALYSIS

While total teleconnectivity reflects the aggregate strength of all teleconnection patterns pertinent to a location, PC analysis explicitly identifies the strongest individual patterns contributing to the total teleconnectivity throughout the domain. Rotated PC solutions usually provide simpler, more localized, and more physically interpretable modes than unrotated solutions

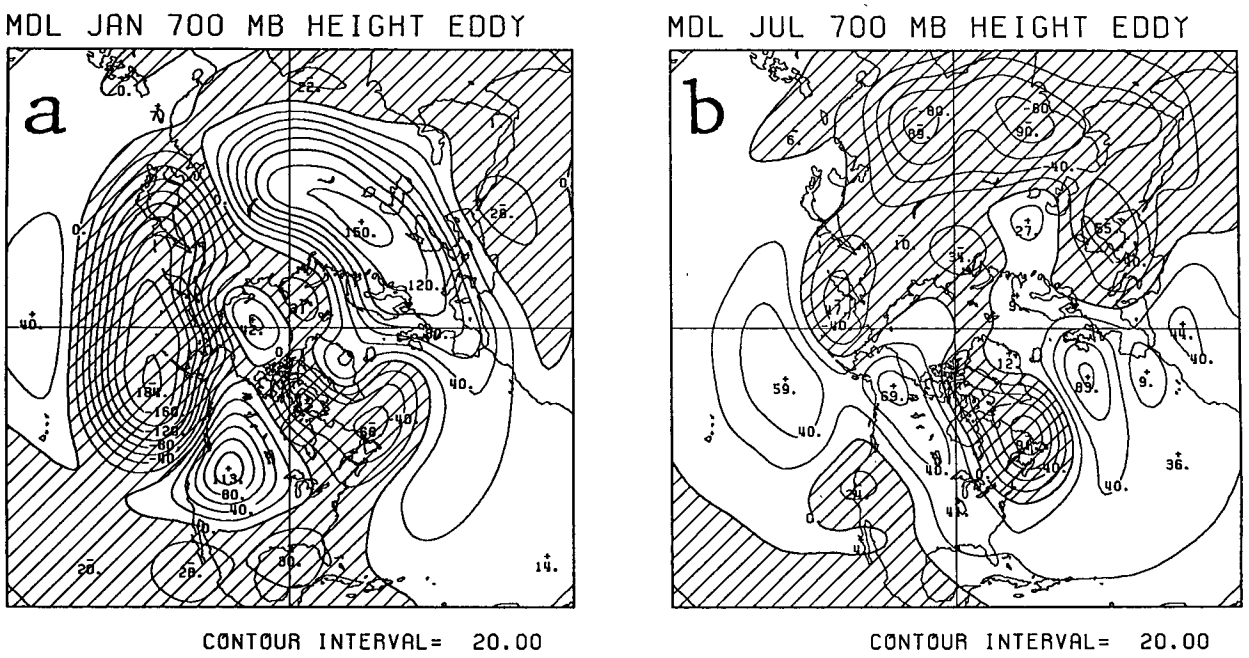

FIG. 12. The eddy component of the MRF model's 10-year-mean 700-mb height (gpm) for (a) January and (b) July. Contour interval is 20 gpm.

(Horel 1981; Richman 1986; Barnston and Livezey 1987). Rotated solutions are also more closely related to the major teleconnection patterns (Namias 1981; Wallace and Gutzler 1981; Esbensen 1984; Richman and Lamb 1985).

Figure 11 shows areas within which the leading 10 varimax-rotated PCs (using a correlation matrix) are loaded most heavily—that is, with at least a 0.6 magnitude of correlation between the principal component time series and the original gridpoint data—for January (part a) and July (part b) unpooled data. The mode number is indicated at the location of strongest loading magnitude, with an exclamation point if it is 0.8 or higher; minus signs are used to denote polarity with respect to other centers of multicenter patterns. The stippled areas do not have any 0.45 or greater loadings among the leading 10 modes. Many of the Fig. 11 patterns are identifiable in the teleconnection and rotated PC literature cited above (e.g., January mode 3 is the PNA pattern). The location of each of the three sites of maximum standard deviation are shown by the A (Atlantic), P (Pacific), and Ar (Arctic). The first 10 modes account for 80 percent of the total variance in January, and 65 percent in July.

In January the Atlantic maximum variability site is within (but not in the middle of) a strong center of the leading mode (the west Atlantic pattern), the Pacific site is near the middle of the strongest center of mode 3 (the PNA pattern), and the Arctic site is near the middle of the monopole northern Asian pattern (mode 6). In the latter two cases a strong association with the coinciding rotated PC pattern is possible, while for the Atlantic site this appears less likely. There are also strong PC pattern centers at similar latitude that are not associated with a high-variability site (e.g., mode 4 west of Scandinavia, mode 3 in southwestern Canada). The variability minimum from the southwestern United States to the Great Lakes coincides with an area lacking in strong rotated PC activity. Inspection of the July correspondences (Fig. 11b) shows a lack of coincidence of strong mode centers and high-variability sites for the Atlantic and Pacific sites and a clear coincidence of the Arctic site with a center of mode 4. While the Atlantic and Pacific sites do not move very much from winter to summer, the rotated PC patterns residing over these oceans undergo major changes (Barnston and Livezey 1987); in fact, there is no summer PNA pattern. This in itself suggests that the PCs are not closely related to the high-variability sites—that is, that the partial congruence of the two in winter may be accidental. The leading 10 modes are found to explain only 55 percent of the July variance at the Pacific peak variability site and 56 percent at the Atlantic site (compared with 65 percent for the hemisphere as a whole), underscoring the role of "random variability" (or feedback interactions from local boundary conditions) at those locations in summer. The Arctic site, on the other hand, migrates across the North Pole to the western hemisphere in summer, coinciding with the disappearance of the winter northern Asian pattern and the emergence of the mode 4 July pattern whose Arctic Ocean center becomes a preferred residence for highest Arctic variability. At this location 70 percent of the July variance is explained by the first 10 modes, 40 percent of which is due to mode

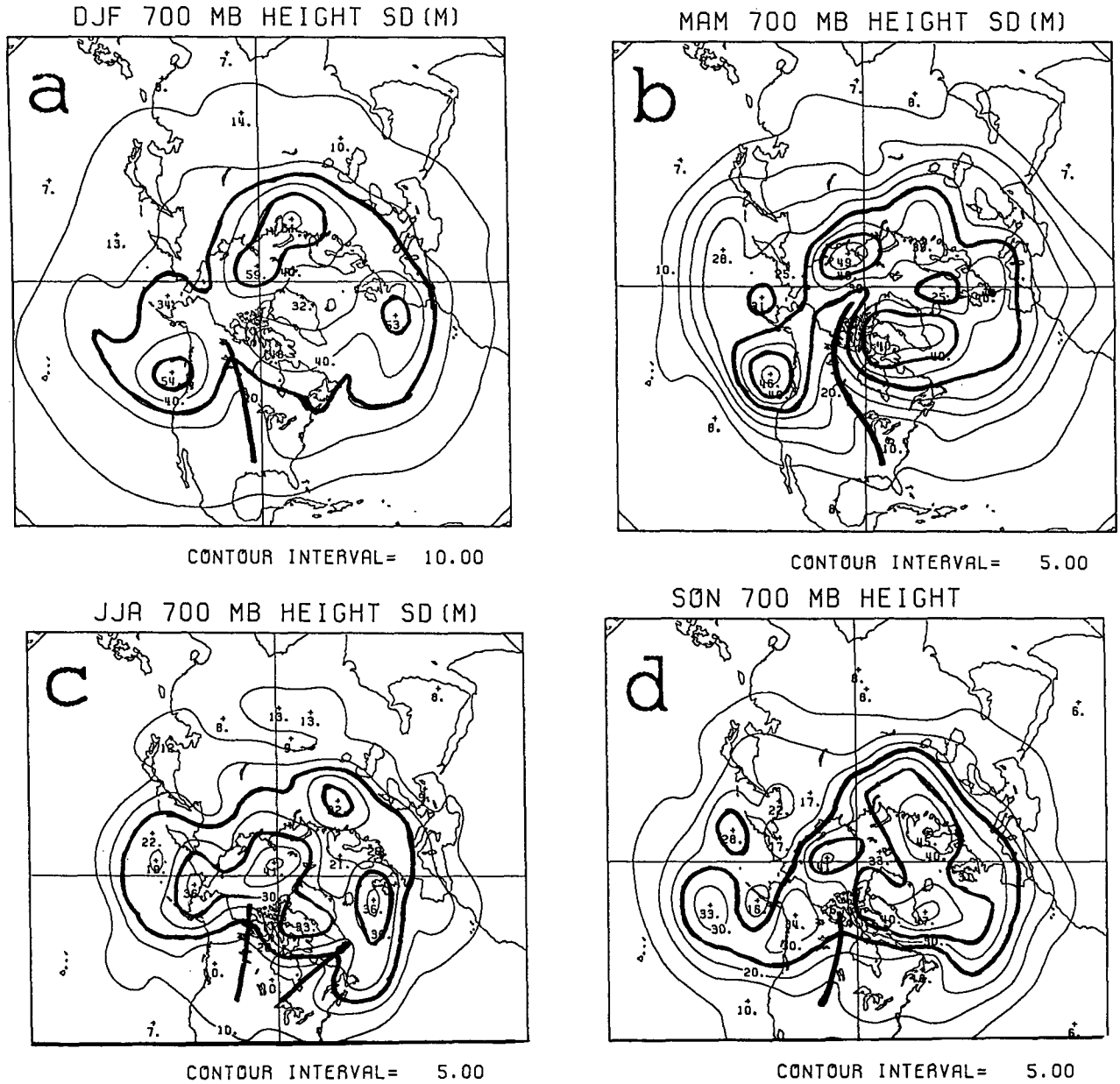

FIG. 13. Geographic distribution of the interannual standard deviation (gpm) of monthly mean model 700-mb height over the 10-year MRF model integration period for (a) January, (b) April, (c) July, and (d) October. Pooling of the standard deviation over the three-month period centered at the target month has been done to reduce sampling variability. Contour interval is 10 gpm for January, 5 gpm for the others. Benchmark contours are darkened as an interpretive aid, and the axis of minimum standard deviation in North America is highlighted.

4. The western North American variability minimum line in July is positioned along the eastern edge of mode 5's western center.

Based on January, July, and some of the intervening months (not shown), there appears to be some relationship between the locations of rotated PC loading pattern centers and the sites of maximum interannual standard deviation. Areas of minimum standard deviation have a correspondingly greater likelihood of occurring in between the PC centers. However, the relationship is not strong, allowing for numerous exceptions. The high-variability centers are often not explained by a single PC mode; this is true to an even greater extent with the larger-scale unrotated PCs (not shown). The PC patterns are considerably more seasonally dependent than the sites of maximum variability, suggesting that the latter are more closely linked to the permanent features of the lower boundary—ocean versus land, and orography—and less to the mean flow, which is completely different in winter than in summer.

Based on mean teleconnectivity and PC analysis, we conclude that membership of the peak variability regions in coherent low-frequency variability patterns is possible but not required. In fact, *connectedness is conspicuously absent in summer.* The leading coherent low-frequency variability patterns, collectively, largely constitute the interannual standard deviation fields but do not tend to correspond to specific variability peaks individually. Not incompatible with this finding is the fact that the correlation between the heights at any two of the three maximum variability sites *is poor at all times of the year.* Apparently there is a strong local or regional component in the interannual variability of monthly mean 700-mb height at these sites.

6. Reproducibility in a general circulation model

A testing of the hypothesis of a relationship between the earth's fixed boundary conditions and the mean and variability of the atmospheric flow patterns can be conducted with general circulation models that are endowed with sufficient resolution and physics. A candidate model is the NMC global spectral medium-range forecast (MRF) model, containing 18 vertical levels and T40 horizontal resolution. The MRF model has been experimentally integrated over a 10-year period in a recent study intended to determine whether NMC's numerical weather forecast model can reproduce the basic features of the earth's climate at very long projection times (Van den Dool et al. 1991; Van den Dool and Saha 1993). The model was integrated from 31 July 1990 conditions. Boundary conditions included solar radiation that changed daily according to the astronomical calendar, and snow depth, soil moisture, sea-ice and sea surface temperature that changed daily according to their climatologies. We now discuss the outcome of the extended run.

The eddy component of the model's 10-year-mean 700-mb height is shown for January and July in Fig. 12, which we discuss in conjunction with its observed counterpart (Fig. 2). Both model and reality have a year-round ridge over western North America, a trough over eastern Canada, and a ridge over the east Atlantic and western and northern Europe. Very large seasonal changes are noted in the deep wintertime low in the Pacific which turns into a high in summer in both model and reality. Another well simulated seasonal contrast is found over central southern and eastern Asia. On the whole the simulated July map is very good. The January model results are mediocre in that the deep Pacific low is about 90° longitude too far east, and associated smaller shifts in most other major features are present. Overall, however, the good approximate agreement gives credence to the idea that the gross boundary features, whose physical implications are roughly accounted for in the model, determine the general nature of the departures from the zonal-mean flow.

The standard deviation of monthly mean 700-mb height based on the model are shown in Fig. 13, which we discuss here in conjunction with Fig. 3, its observed counterpart. Even with the pooling of three adjacent months the model still has only 30 realizations from which to calculate the standard deviation. Using the method detailed in section 4 to estimate confidence intervals for the population standard deviation in terms of the sample standard deviation s, it is found that with 30 cases the 95 percent confidence interval spans from $0.80s$ to $1.34s$. Thus sampling errors are not negligible; however, some model features clearly stand out despite the uncertainty. Model and reality agree that variability increases with latitude in all seasons. Also the seasonality is correct in that monthly means show highest (lowest) variability in winter (summer), and spring has slightly higher variability than fall. Both model and reality place the maxima of variability in the Arctic, the two northern oceans, and northern Asia. The location of the axis of minimum variability over North America is well simulated. There is also agreement in the complete absence of any north–south seasonal shifting in the latitude band of maximum variability. There are considerable disagreements in all seasons between model and observed fields on the precise location of variability maxima. In part this may be a sampling problem (i.e., we did not run the model long enough). In winter the model variance maxima appear shifted eastward relative to the observed maxima, similar to the mean flow itself. Therefore the relationship between mean flow and eddies may still be the same in the model as in reality.

There is a large discrepancy in the magnitude of the standard deviation. The model standard deviation is typically only two-thirds of the observed; that is, in terms of variance, less than half. We believe this is a serious model deficiency that will be ameliorated to some extent by providing the model with interannually varying lower boundary conditions. There is a similar lack of variance in the high-frequency eddies (not shown). There is also a discrepancy in that in reality the Pacific peak is locationally constant while in the model it wanders considerably over the seasons.

7. Discussion

An atlas of monthly mean statistics of Northern Hemisphere 700-mb height for the 1950–1991 period is published for the convenience of atmospheric researchers and operational meteorologists and climatologists. This paper highlights and extends some of the more interesting or central features of these compiled data and makes a comparison to the statistics of a 10-year run of the NMC medium-range forecast model.

Fields of the Northern Hemisphere interannual standard deviation of monthly mean 700-mb height through the annual cycle reveal three general regions

of peak standard deviation. Two of these regions are in the east central portion of the high-latitude Pacific and Atlantic oceans, respectively, and the third is over the Arctic Ocean or adjacent northwestern Soviet Union. The latter region exhibits a seasonal migration pattern, moving to the opposite (Alaskan) side of the pole during the summer months and farthest south into northwestern Russia in midfall through early winter. A north-to-south troughlike minimum in standard deviation is found in west-central North America most of the year, providing an optimal site for studying phenomena of still lower frequency without the obscuring effects of the "regular" low-frequency noise.

There are three general findings regarding the behavior of the standard deviation peaks in monthly mean 700-mb height. The first is that they are fairly closely associated with high frequencies of occurrence of centers of positive and negative anomalies in monthly mean flow, and the variability minima with a relative absence of such. While strong positive outliers are more likely than their negative counterparts (causing a positive skewness coefficient), marked asymmetry, in a broader sense, is not generally found in the anomaly distributions, indicating that anomalies of either sign are about equally likely.

The second general result is that there is a noticeable but only rather weak tendency for the high variability regions to belong to a collection of spatially coherent variability clusters (i.e., multicenter patterns, as would be reflected in teleconnection statistics) more than other regions in the extratropical Northern Hemisphere. Their involvement in the clusters is considerably greater in terms of data variance, but only slightly so in terms of the strength of the relationships—and only in the cold season. In fact, *in summer the association between the high-variability regions and the coherent variability clusters is conspicuously weak.*

Finally (and perhaps most remarkably) is the observation, related to the second result, that the locations of the three variability maxima do not exhibit a north–south seasonal migration as do the jet streams and cyclone tracks to their south. The Pacific high-variability site, in particular, remains quite tightly anchored near 50°N, 170°W throughout the year regardless of substantial seasonal changes in this region in the mean flow and in the coherent patterns of low-frequency variability as depicted by teleconnections or PC analysis. These observations suggest that the main characteristics of the standard deviation field are caused to a significant extent by local interactions (which appear random with respect to the coherent variability patterns). These interactions, we think, are closely related to the permanent features of the lower boundary, such as ocean versus land, and orography.

The observed monthly mean 700-mb flow and the quasi-stationary locations of its interannual standard deviation maxima and minima are reproduced in approximate form in a 10-year run of the NMC medium-range forecast model. The zonal-mean and eddy components of the flow are reproduced fairly well, suggesting that the gross boundary features roughly determine the nature of the departures from the zonal-mean flow. The maxima in the standard deviation field, while somewhat displaced from those observed, do occur in the Arctic, the two northern oceans, and northern Asia. The axis of minimum variability in North America is well simulated. As in reality, there is no north–south seasonal migration of the latitude of maximum variability. These findings help provide evidence that the field of standard deviation is related, directly or indirectly, to some of the geographically fixed boundary conditions across the globe such as SST, ocean–land interfaces, and terrain.

Acknowledgments. The authors wish to thank Drs. Jeffrey Anderson, Ming Cai, and A. James Wagner for their careful reviews of an earlier version of this paper.

REFERENCES

Anderson, J. L., 1991: The robustness of barotropic unstable modes in a zonally varying atmosphere. *J. Atmos. Sci.*, **48,** 2393–2410.

——, 1992: Barotropic stationary states and persistent anomalies in the atmosphere. *J. Atmos. Sci.*, **49,** 1709–1722.

Barnston, A. G., and R. E. Livezey, 1987: Classification, seasonality and persistence of low-frequency atmospheric circulation patterns. *Mon. Wea. Rev.*, **115,** 1083–1126.

——, and H. M. van den Dool, 1993: *Atlas of Climatology and Variability of Monthly Mean Northern Hemisphere Sea Level Pressure, 700 mb Geopotential Height, and 1000–700 mb Thickness,* 1950–1992. NOAA Atlas No. 10, Camp Springs, MD, 219 pp.

Bernardet, P., A. Butet, M. Deque, M. Ghil, and R. L. Pfeffer, 1990: Low-frequency oscillations in a rotating annulus with topography. *J. Atmos. Sci.*, **47,** 3023–3043.

Blackmon, M. L., Y.-H. Lee, and J. M. Wallace, 1984: Horizontal structure of 500-mb height fluctuations with long, intermediate, and short time scales. *J. Atmos. Sci.*, **41,** 961–979.

Branstator, G., 1987: A striking example of the atmosphere's leading traveling pattern. *J. Atmos. Sci.*, **44,** 2310–2323.

——, and J. D. Opsteegh, 1989: Free solutions of the barotropic vorticity equation. *J. Atmos. Sci.*, **46,** 1799–1814.

Byers, H. R., 1974: *General Meteorology.* Fourth Edition. McGraw-Hill, Inc., 461 pp.

Cai, M., and M. Mak, 1990: Symbiotic relation between planetary and synoptic-scale waves. *J. Atmos. Sci.*, **47,** 2953–2968.

——, and H. M. van den Dool, 1991: Low-frequency waves and traveling storm tracks. Part I: Barotropic component. *J. Atmos. Sci.*, **48,** 1420–1436.

Cane, M. A., and S. E. Zebiak, 1987: Prediction of El Niño events using a physical model. *Atmospheric and Oceanic Variability,* H. Cattle, Royal Meteorological Society, Ed. James Glaisher House, 153–181.

Douglas, A. V., D. R. Cayan, and J. Namias, 1982: Large-scale changes in North Pacific and North American weather patterns in recent decades. *Mon. Wea. Rev.*, **110,** 1851–1862.

Esbensen, S. K., 1984: A comparison of intermonthly and interannual teleconnections in the 700 mb geopotential height field during the Northern Hemisphere winter. *Mon. Wea. Rev.*, **112,** 2016–2032.

Hays, W. L., 1973: *Statistics for the Social Sciences,* Holt, Rinehart and Winston, Inc., 954 pp.

Horel, J. D., 1981: A rotated principal component analysis of the interannual variability of the Northern Hemisphere 500-mb height field. *Mon. Wea. Rev.*, **109,** 2080–2092.

Hsu, C.-P. F., and J. M. Wallace, 1976: The global distribution of the annual and semiannual cycles in sea level pressure. *Mon. Wea. Rev.*, **104,** 1597–1601.

Jin, F.-F., and M. Ghil, 1990: Intraseasonal oscillations in the extratropics: Hopf bifurcation and topographic instabilities. *J. Atmos. Sci.*, **47,** 3007–3022.

Klein, W. H., 1957: Principal tracks and mean frequencies of cyclones and anticyclones in the Northern Hemisphere. Research Paper No. 40, Department of Commerce, Extended Forecast Section, 60pp. [Available from W. H. Klein, Department of Meteorology, University of Maryland, College Park, MD 20742.]

——, 1983: Objective specification of monthly mean surface temperature from mean 700-mb heights. *Mon. Wea. Rev.*, **111,** 674–691.

——, and J. E. Walsh, 1983: A comparison of point-wise screening and empirical orthogonal functions in specifying monthly surface temperatures from 700 mb data. *Mon. Wea. Rev.*, **111,** 669–673.

Lanzante, J. R., 1990: The leading modes of 10–30-day variability in the extratropics of the Northern Hemisphere during the cold season. *J. Atmos. Sci.*, **47,** 2115–2140.

Lau, N.-C., and M. J. Nath, 1991: Variability of the baroclinic and barotropic transient eddy forcing associated with monthly changes in the midlatitude storm tracks. *J. Atmos. Sci.*, **48,** 2589–2613.

Madden, R. A., 1976: Estimates of the natural variability of time-averaged sea-level pressure. *Mon. Wea. Rev.*, **104,** 942–952.

——, and P. R. Julian, 1971: Detection of a 40–50 day oscillation in the zonal wind in the tropical Pacific. *J. Atmos. Sci.*, **28,** 702–708.

Namias, J., 1952: The annual course of month-to-month persistence in climatic anomalies. *Bull. Amer. Meteor. Soc.*, **33,** 279–285.

——, 1981: Teleconnections of 700 mb height anomalies for the Northern Hemisphere. *Calcofi Atlas No. 29,* A. Fleminger, Ed., Marine Life Research Program, Scripps Institution of Oceanography, 265 pp.

O'Connor, J., 1969: Hemispheric teleconnections of mean circulation anomalies at 700 millibars. ESSA Technical Report WB10, U.S. Department of Commerce, Silver Spring, MD, 103 pp.

Opsteegh, J. D., and H. M. van den Dool, 1980: Seasonal differences in the stationary response of a linearized primitive equation model: Prospects for long range weather forecasting? *J. Atmos. Sci.*, **37,** 2169–2185.

Reinhold, B. B., and R. T. Pierrehumbert, 1982: Dynamics of weather regimes: Quasi-stationary waves and blocking. *Mon. Wea. Rev.*, **110,** 1105–1145.

Richman, M. B., 1986: Rotation of principal components. *J. Climatol.*, **6,** 293–335.

——, and P. J. Lamb, 1985: Climatic pattern analysis of three- and seven-day rainfall in the central United States: Some methodological considerations and a regionalization. *J. Climate Appl. Meteor.*, **24,** 1325–1343.

Ropelewski, C. F., and M. S. Halpert, 1986: North American precipitation and temperature patterns associated with the El Niño/Southern Oscillation (ENSO). *Mon. Wea. Rev.*, **114,** 2352–2362.

Simmons, A. J., J. M. Wallace, and G. W. Branstator, 1983: Barotropic wave propagation and instability, and atmospheric teleconnection patterns. *J. Atmos. Sci.*, **40,** 1363–1392.

Trenberth, K. E., 1990: Recent observed interdecadal climate changes in the Northern Hemisphere. *Bull. Amer. Meteor. Soc.*, **71,** 988–993.

Van den Dool, H. M., and R. E. Livezey, 1984: Geographical distribution and seasonality of month-to-month correlation of monthly mean 700-mb heights. *Mon. Wea. Rev.*, **112,** 610–615.

——, and S. Saha, 1993: Seasonal redistribution and conservation of atmospheric mass in a general circulation model. *J. Climate,* **6,** 22–30.

——, ——, and Z. Toth, 1991: The climate in a multi-year NMC model run. *Proc. Fifth Conference on Climate Variations,* Denver, Colorado, October 14–18, 511–514.

Wagner, A. J., and T. N. Maisel, 1988: Northern Hemisphere 700 mb teleconnections based on half-monthly mean anomaly data stratified by season and by sign. *Proc. of the 12th Annual Climate Diagnostics Workshop,* Salt Lake City, Utah, Amer. Meteor. Soc., 228–237.

Wallace, J. M., 1987: Low-Frequency Dynamics—Observation. Notes from an NCAR Summer Colloquium: "Dynamics of Low-Frequency Phenomena in the Atmosphere. Vol. I: Observations", NCAR. 1–75. [Available from NCAR, Boulder, CO 80303.]

——, and D. S. Gutzler, 1981: Teleconnections in the geopotential height field during the Northern Hemisphere winter. *Mon. Wea. Rev.*, **109,** 784–812.